ACADEMIC PRESS

Available online at www.sciencedirect.com
SCIENCE DIRECT®

Journal of Catalysis 216 (2003) 203–212

JOURNAL OF CATALYSIS

www.elsevier.com/locate/jcat

Identifying the isolated transition metal ions/oxides in molecular sieves and on oxide supports by UV resonance Raman spectroscopy

Can Li

State Key Laboratory of Catalysis, Dalian Institute of Chemical Physics, Chinese Academy of Sciences, Dalian 116023, China

Received 8 July 2002; revised 3 September 2002; accepted 17 September 2002

Abstract

Isolated transition metal ions/oxides in molecular sieves and on surfaces are a class of active sites for selective oxidation of hydrocarbons. Identifying the active sites and their coordination structure is vital to understanding their essential role played in catalysis and designing and synthesizing more active and selective catalysts. The isolated transition metal ions in the framework of molecular sieves (e.g., TS-1, Fe-ZSM-5, and V-MCM-41) or on the surface of oxides (e.g., MoO_3/Al_2O_3 and TiO_2/SiO_2) were successfully identified by UV resonance Raman spectroscopy. The charge transfer transitions between the transition metal ions and the oxygen anions are excited by a UV laser and consequently the UV resonance Raman effect greatly enhances the Raman signals of the isolated transition metal ions. The local coordination of these ions in the rigid framework of molecular sieves or in the relatively flexible structure on the surface can also be differentiated by the shifts of the resonance Raman bands. The relative concentration of the isolated transition metal ion/oxides could be estimated by the intensity ratio of Raman bands. This study demonstrates that the UV resonance Raman spectroscopy is a general technique that can be widely applied to the in-situ characterization of catalyst synthesis and catalytic reactions.

Keywords: UV Raman; Resonance Raman; Spectroscopy; Isolated transition metal ions; Transition metal oxides; Selective oxidation; Active sites; Catalysts

1. Introduction

1.1. UV Raman spectroscopy applied to catalyst characterization

Raman spectroscopy is an important spectroscopic technique and is considered to be a powerful tool for characterizing molecular structures. It has been extensively applied to the study of chemistry, physics, biology, and material science [1]. The visible lasers are usually used as the excitation sources for conventional Raman spectroscopy. Unfortunately, the fluorescence and some other background interference (hereafter referred to as fluorescence) frequently occur in the visible or near-UV region. The intensity of the fluorescence is usually higher than that of a Raman signal by several orders of magnitude. As a result, the visible Raman spectra are often obscured by the strong fluorescence. Another shortcoming of conventional Raman spectroscopy is the inherently low Raman scattering intensity.

It has been a challenging and important task to make Raman spectroscopy widely applicable to the study of catalysis because Raman spectroscopy is potentially more useful for in-situ study of working catalysts. However, the fluorescence is extremely severe for catalysts mainly due to the fluorescence impurity frequently present on catalyst surfaces. In particular, the hydrocarbon species, such as organic template residues in zeolites, produce the strong fluorescence. These species are inevitably formed on the surfaces of catalysts under reaction conditions. It is difficult to obtain Raman spectra once the samples have fluorescence. Therefore, avoiding or eliminating the fluorescence and increasing the sensitivity are the most significant ways to apply Raman spectroscopy to catalysis, materials science, and many other fields.

The fluorescence spectrum varies for different catalysts, but most spectra lie in the range from 300 to 700 nm or longer as shown in Fig. 1. The fluorescence band may extend to the visible and near-infrared regions, but there is a cut-off wavelength in the shorter wavelength side, usually in the UV region. Most samples are totally free of fluorescence in the region shorter than approximately 260 nm. This can

E-mail address: canli@dicp.ac.cn.
URL address: http://www.canli.dicp.ac.cn.

0021-9517/03/$ – see front matter
doi:10.1016/S0021-9517(02)00107-0

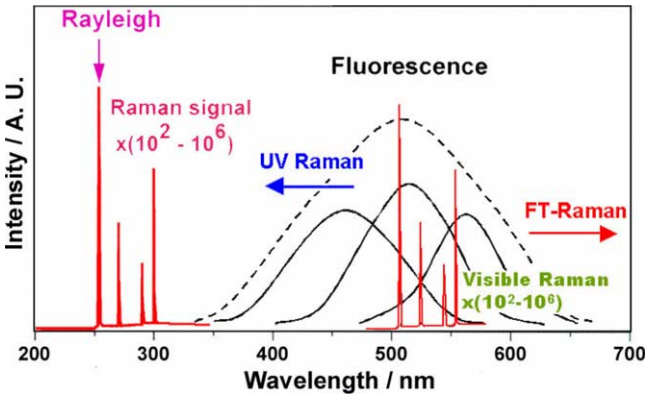

Fig. 1. To avoid fluorescence interference, the excitation laser is shifted from the visible region to the UV region ($\lambda < 300$ nm), which is nearly fluorescence free. The fluorescence bands appear mostly in the visible region from about 300 to 700 nm, and the Raman signal is usually about 10^2–10^6 less intense than the fluorescence signal.

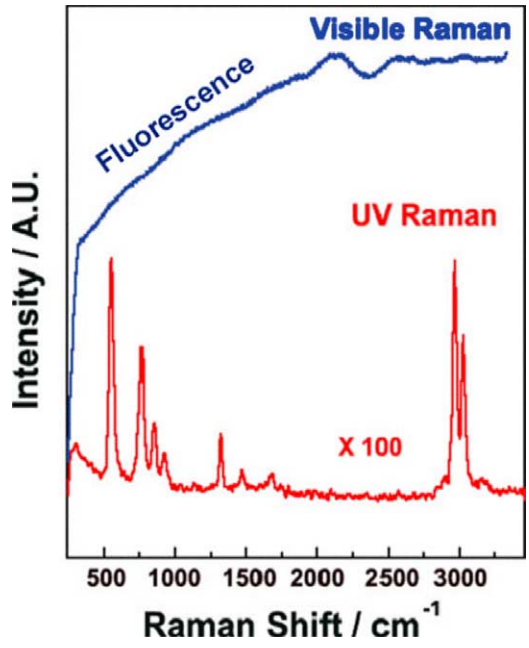

Fig. 2. A comparison between the visible Raman spectrum ($\lambda_{ex} = 488$ nm) and UV Raman spectrum ($\lambda_{ex} = 244$ nm) of silicon grease used for vacuum sealing. The silicon grease gives strong fluorescence, and its Raman signals are submerged in the broad background in the visible Raman spectrum. The Raman bands of grease clearly appear in its UV Raman spectrum, indicating that the strong fluorescence of grease is effectively avoided by shifting the excitation laser from the visible region to the UV region.

be explained because the fluorescence is produced mainly from the transition from the first excited electronic state to the vibrational states of the ground electronic state, and this band gap for most catalysts is in the visible region. Therefore, it is possible to avoid the fluorescence by shifting the excitation laser from the visible region to the UV region as described in Fig. 1.

Recent UV Raman spectroscopic studies on various catalysts demonstrated that the fluorescence interference could be successfully avoided in UV Raman spectroscopy [2–5]. Fig. 2 shows an example of silicon grease, which usually has strong fluorescence and is frequently plagued by the fluorescence problem, when a Raman cell was sealed with it. The two spectra clearly suggest that the fluorescence can be avoided in the Raman spectra when the Raman spectra are placed in the UV region. Similar results were obtained for zeolites [6], alumina [7], coked catalysts [8], etc. In principle the sensitivity of Raman spectroscopy can be further increased by shifting the excitation laser from the visible region to the UV region, since the Raman scattering intensity is inversely proportional to λ^4 (where λ is the wavelength of the Raman scattering).

Another merit of UV Raman spectroscopy is that the resonance Raman spectra can be obtained for some samples by exciting the electronic states with an ultraviolet laser, since the electronic transition of chemical compounds usually occurs in the UV region. The Raman scattering intensity is proportional to $|\alpha_{\rho\sigma}|^2$, and the polarizability ($\alpha_{\rho\sigma}$) can be calculated according to the Kramers–Heisenberg equation [9],

$$(\alpha_{\rho\sigma})_{mn} = \frac{1}{h}\sum\left(\frac{M_{me}M_{en}}{\Delta E_{me} - h\nu_0 + i\Gamma} + \frac{M_{me}M_{en}}{\Delta E_{en} + h\nu_0 + i\Gamma}\right),$$

where the ν_0 is the frequency of excitation laser, ΔE_{me} stands for the energy difference between the two electronic states, m and e, while state n is the first excited vibrational energy level. The polarizability ($\alpha_{\rho\sigma}$) would be greatly increased when the laser line ($h\nu_0$) is close to an electronic transition (ΔE_{me}). As a result, the cross section of Raman scattering could be considerably enhanced. This enhancement in intensity could be several orders of magnitude greater than the normal Raman intensity. Therefore resonance Raman spectroscopy is a useful tool to discern information from a complex molecular system, especially information about the local structure of a complex system such as catalysts.

One should be careful when the UV Raman spectra of some photosensitive catalysts are measured because the UV laser may induce photodecomposition of the surface species on the catalyst and catalyst itself. But most inorganic compounds such as SiO_2, Al_2O_3, and zeolites are quite stable under UV radiation (the laser power was kept at less than 5 mW in this work to alleviate the thermal effect).

1.2. Detection of isolated transition metal ions by UV resonance Raman spectroscopy

Fig. 3 describes how one can apply resonance Raman spectroscopy to the identification of isolated transition metal ions incorporated in the framework of molecular sieves. For the transition metal ion (M) isolated in a silicalite-like matrix, there is a charge transfer transition between the framework oxygen anion and the framework transition metal cation. This transition is mostly located in the UV region,

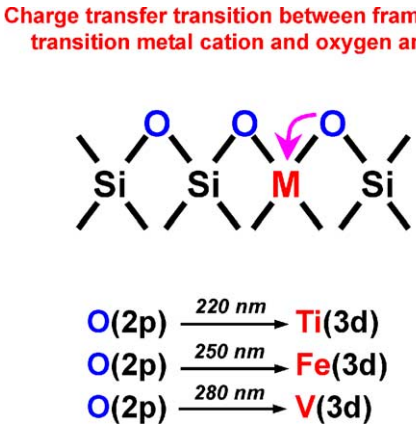

Fig. 3. Isolated transition metal ions in the framework of zeolites, such as Ti in TS-1. The charge transfer transition between the framework transition metal cation and the oxygen anion falls in the UV region for most cases.

e.g., 220 nm for TS-1, 250 nm for Fe-ZSM-5, and 280 nm for V-MCM-41. In this manner, we can take advantage of the UV resonance Raman effect to detect/identify the isolated framework transition metal ions in molecular sieves.

Molecular sieves with incorporated transition metal ions in their framework are a new class of materials that show important properties in catalysis. The most useful property is their redox ability that can be used as new catalysts for selective oxidation of a wide range of hydrocarbons, such as the epoxidation of olefins and hydroxylation of benzene using H_2O_2 as the oxidant [10,11]. The most interesting question concerning the incorporated transition metal ions in molecular sieves is how to identify the transition metal ions in the framework.

The transition metal ions substituted in the framework of molecular sieves show a charge transfer transition, usually in the UV region, between the transition metal ions and the framework oxygen anions. Therefore the UV resonance Raman spectra can be obtained by exciting these transitions with the UV laser. Accordingly, the framework transition ions can be selectively identified based on the resonance Raman effect because the enhanced resonance Raman bands are directly associated with the framework transition metal ions.

Isolated and highly dispersed transition metal ions/oxide on oxide supports (e.g., Al_2O_3 and SiO_2) are frequently the active sites or the phases of catalysts for many kinds of reactions including the selective oxidation of hydrocarbons [12,13]. Similar to the transition metal ions substituted in molecular sieves, the characterization of the active sites in isolated and highly dispersed forms is also important in gaining insight into their catalytic natures. There are some similarities in structure between the isolated transition metal ions substituted in molecular sieves and the isolated/dispersed transition metal oxides on supports. The isolated/dispersed transition metal oxide species on supports can be also identified by UV resonance Raman spectroscopy.

In this paper, three typical molecular sieves (TS-1, Fe-ZSM-5, and V-MCM-41) and two typical supported transition metal oxides (MoO_3/Al_2O_3 and TiO_2/SiO_2) are characterized by UV resonance Raman spectroscopy. The isolated transition ions/oxide in these molecular sieves and on oxide supports are clearly identified based on the UV resonance Raman effect.

2. Isolated transition metal ions incorporated in molecular sieves

2.1. Isolated titanium sites in the framework of TS-1

TS-1 zeolite has received a great deal of attention in the past decade because of its excellent catalytic properties in a range of selective oxidation reactions with aqueous hydrogen peroxide as the oxidant under mild conditions. It is commonly believed that isolated titanium in the framework of the TS-1 zeolite, hereafter denoted by Ti–O–Si, is the active site for the selective oxidation, although the exact nature of the active site is still under dispute. There has been extensive characterization of the TS-1 zeolite using various techniques such as FT–IR, Raman spectroscopy, UV–visible absorption, NMR, EXAFS and XANES, XRD, neutron powder diffraction, etc. [14–21]. A band that appeared at 960 cm^{-1} in Raman and IR spectra was assumed to be the characteristic vibration mode of the framework titanium species, Ti–O–Si. However, this band sometimes appears for silicalite zeolites without substituted titanium or with substituted metal instead of titanium and there is also evidence indicating that this band may be from surface hydroxyl (e.g., Si–OH) [22,23] or defect sites [24]. Thus the question still remains on how the framework titanium species can be unambiguously identified.

Fig. 4 gives the Raman spectra of TS-1 excited by three different laser lines at 244, 325, and 488 nm. The inset in Fig. 4 shows the UV–visible diffuse reflectance spectra of TS-1 and silicalite. There is a typical absorption band centered at 220 nm for TS-1 while no electronic absorption band is observed for silicalite-1. The band at 220 nm originates from the charge transfer of the $p\pi$–$d\pi$ transition between titanium and oxygen of the framework titanium species, Ti–O–Si, in the zeolite. The tail of the band centered at 220 nm actually extends to 300 nm due to the presence of an extra framework titania species, TiO_2, in the TS-1 zeolite.

The upper spectrum in Fig. 4 is the UV Raman spectrum of TS-1 excited by the 244-nm line [25]. There are strong Raman bands observed for TS-1 at 1125, 960, 815, 530, 490, 380, and 290 cm^{-1} and some weak bands in the 600–800 cm^{-1} region. Of particular interest is a very strong band at 1125 cm^{-1} observed for TS-1 although its bands in the 1000 cm^{-1} region are usually very weak in the normal Raman spectroscopy. The UV Raman spectrum of silicalite-1 is completely different from that of TS-1. The strong Raman bands at 490, 530, and 1125 cm^{-1}, which appear for

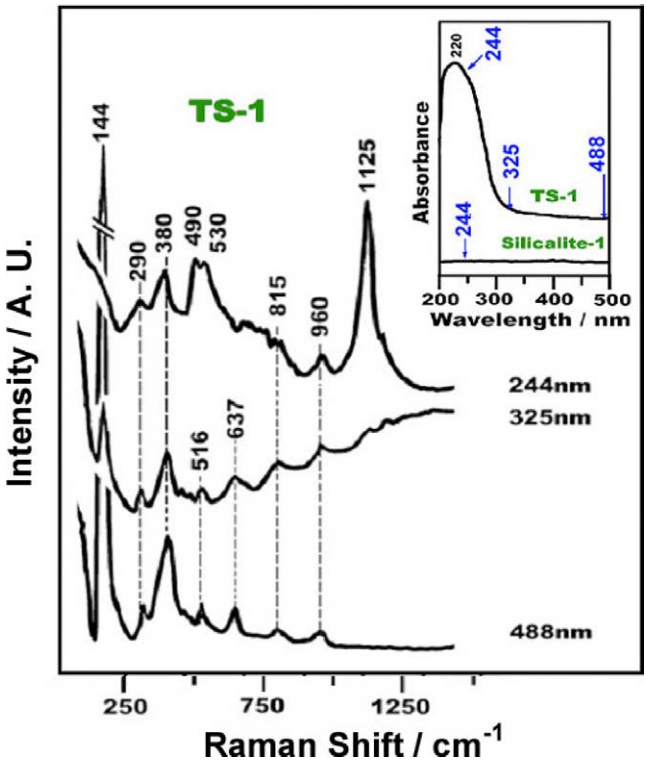

Fig. 4. Raman spectra of TS-1 excited by different lasers at 244, 325, and 488 nm. The inset is the UV-visible diffuse absorbances of TS-1 and silicalite-1. The laser at 244 nm is close to the charge transfer transition of TS-1, but the lasers at 325 and 488 nm are out of the absorbance band of TS-1.

TS-1, are absent in the Raman spectrum of silicalite-1 [26]. These new bands must be from the framework titanium species in TS-1. Several common bands are observed at 290, 380, and 815 cm^{-1} for both TS-1 and silicalite-1 zeolites indicating that these bands are characteristic of the silicalite-1 zeolite. The weak band at 960 cm^{-1} in the UV Raman spectrum appears at the same frequency as that in FT–IR and FT–Raman spectra ($\lambda_{ex} = 1064$ nm).

Fig. 4 compares the Raman spectra of TS-1 excited by three different laser lines at 244, 325, and 488 nm. The strong bands at 490, 530, and 1125 cm^{-1} are observed only when excited with the line at 244 nm. Clearly these bands are due to the UV resonance Raman effect because the 244-nm line is in the absorbance band of the electronic absorption of TS-1 while the 325- and 488-nm lines are outside of the absorption band of TS-1 (see inset). All three spectra have common bands at 290, 380, 815, and 960 cm^{-1}, suggesting that the appearance of these bands may not be due to the resonance Raman effect [26].

The Raman spectra of silicalite-1 excited with lines at 244, 325, and 488 nm are almost identical. The interesting bands at 490, 530, and 1125 cm^{-1} are not detected for silicalite-1 for excitation lines from the visible to ultraviolet regions. There is no resonance Raman phenomenon observed for silicalite-1 as no enhanced Raman bands are detected for silicalite-1 when the excitation line varied from the visible to the UV regions (see inset). This confirms that the bands at 490, 530, and 1125 cm^{-1} are solely associated with the framework titanium of TS-1 but not with silicalite-1 [26].

The Raman bands at 290, 380, and 815 cm^{-1} do not vary with the different excitation lines at 244, 325, and 488 nm, indicating that these bands are the characteristic bands of silicalite-1 itself. Specifically, the band at 380 cm^{-1} is the identification of the MFI structure [27]. These bands also appear for TS-1, suggesting that TS-1 still maintains the main structure of silicalite-1. There are some weak bands in the 1000–1200 cm^{-1} region, which are also due to silicalite-1. These bands become evident when the excitation is shifted from 488 to 244 nm mainly due to less fluorescence in the Raman spectrum when the excitation wavelength is shifted from the visible to the ultraviolet regions.

The resonance enhanced Raman bands at 490, 530, and 1125 cm^{-1} can be simply assigned to a local unit of $[Ti(OSi)_4]$ of TS-1, denoted by Ti–O–Si in this paper. The bands at 490 and 530 cm^{-1} are assigned to the bending and symmetric stretching vibrations of the framework Ti–O–Si species respectively and the band at 1125 cm^{-1} is attributed to the asymmetric stretching vibration of the Ti–O–Si [28,29].

It was assumed that the appearance of the band at 960 cm^{-1} (infrared and Raman) was the indication that the framework titanium species had formed in the TS-1. However, the assignment of this band has proven to be controversial [30]. The relative intensity of this band is almost the same among the different excitation lines (Fig. 4). This clearly indicates that the band is not a resonance-related Raman band. The relative intensity of the band at 960 cm^{-1} remains almost unchanged with the crystallization time [26], suggesting that the band at 960 cm^{-1} may not be directly associated with the framework titanium species of TS-1.

A thorough analysis of the vibrational features of the TS-1 catalyst was conducted by Ricchiardi et al. [31] based on quantitative IR measurements, Raman and UV resonance Raman experiments, quantitative XANES, and quantum chemical calculations on cluster and periodic models. The linear correlation of the intensity of the IR and Raman bands located at 960 and 1125 cm^{-1} and the XANES peak at 4967 eV to the amount of tetrahedral Ti was quantitatively demonstrated. Raman and resonant Raman spectra of silicalite and TS-1 with variable Ti content show main features at 960 and 1125 cm^{-1} associated with titanium insertion into the zeolite framework. The enhancement of the intensity of the 1125 cm^{-1} feature and the invariance of the 960 cm^{-1} feature in UV Raman experiments were discussed in terms of resonant Raman selection rules. Quantum chemical calculations on cluster models $Si[OSi(OH)_3]_4$ and $Ti[OSi(OH)_3]_4$ at the B3LYP/6-31G(d) level of theory provided the basis for the assignment of the main vibrational contributions and for the understanding of Raman enhancement. The resonance-enhanced 1125 cm^{-1} mode is unambiguously associated with a totally symmetric vibration of

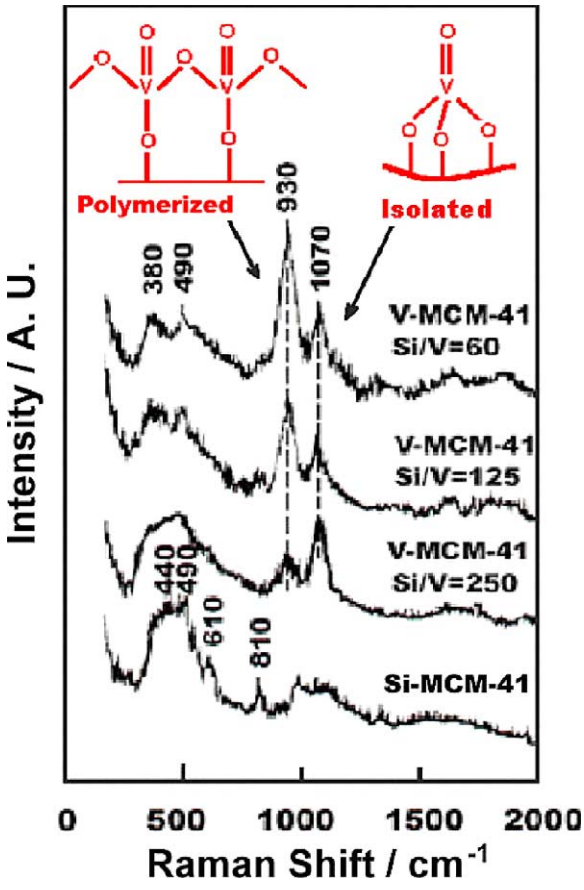

Fig. 5. UV Raman spectra ($\lambda_{ex} = 244$ nm) of V-MCM-41 with different Si/V molar ratios as the starting materials of synthesis.

the TiO_4 tetrahedron, achieved through in-phase asymmetric stretching of the four connected Ti–O–Si bridges.

2.2. Identifying the isolated vanadium sites in V-MCM-41

In the UV–visible reflectance diffuse absorption spectra of Si-MCM-41 and V-MCM-41 [32], no electronic absorption bands are observed for Si-MCM-41, and there are weak electronic absorptions at 270, 340, 410, and 450 nm for V-MCM-41. The electronic absorptions at 270 and 340 nm can be attributed to the charge transfer between the tetrahedral oxygen ligands and the central V^{5+} ion of tetrahedral coordinated V^{5+} in the framework [33–35]. Two bands at 410 and 450 nm indicate that the extra framework V^{5+} ions are formed in V-MCM-41. However, the UV–vis electronic absorption of polymerized vanadium oxides supported on SiO_2 also appears in the 250–350 nm region [36]. The bands at 250 and 320 nm are observed in UV–visible diffused reflectance spectrum of supported vanadium oxides. Hence, the broad bands at 270 and 340 nm are the overlap of the UV–vis bands of both isolated tetrahedral (called framework vanadium, actually formed at the surface defect site with several Si–OH) and polymerized (called extra framework) vanadium sites. The laser line at 244 nm is simultaneously close to the electronic absorption of the vanadium ions in both the isolated and polymerized forms.

Similarly, the vanadium species in V-MCM-41 can be characterized by UV resonance Raman spectroscopy. Fig. 5 shows the UV Raman spectra of Si-MCM-41 and V-MCM-41 excited by the 244-nm line. Visible Raman spectrum of V-MCM-41 illustrates Raman bands similar to those of the MCM-41 and no strong Raman bands associated with the vanadium species in the isolated and polymerized forms. In the UV Raman spectrum two new bands at 930 and 1070 cm^{-1} are detected. The band at 930 cm^{-1} is assigned to the V=O symmetric stretching mode of the polymerized vanadium oxides in the extra framework [37]. The band at 1070 cm^{-1} is assigned to the V=O symmetric stretching mode of the vanadium ions in the isolated form (framework). Considering that the 244-nm line is close to the charge transfer absorption of the vanadium ions, it is the Raman resonance effect that considerably enhances the bands at 930 and 1070 cm^{-1}.

The V=O vibrations of VOX_3 (X = F, Cl, Br) are below 1055 cm^{-1} [38], and that of supported monometric vanadyl species usually gives a band at about 1030 cm^{-1} [39]. The framework vanadium species in V-MCM-41 is in the distorted tetrahedral form as evidenced by the much higher band position at 1070 cm^{-1}. This tetrahedral structure might have strong structural tension, and it is actually a metastable structure that easily aggregates into the polymerized species at higher temperatures. This was confirmed by the experiments proving that the band at 930 cm^{-1} grows while the band intensity at 1070 cm^{-1} decreases when the V-MCM-41 was calcined at elevated temperatures. The intensities of the bands at 1070 and 930 cm^{-1} represents the surface concentration of isolated (framework) and polymerized (extraframework) vanadium species, respectively. Decreasing the Si/V ratio, or increasing the vanadium amount, causes the band intensity at 1070 cm^{-1} due to isolated vanadium species to slightly decrease while the band at 930 cm^{-1} due to polymerized vanadium species increases. The amount of framework vanadium in the V-MCM-41 seems to be limited. When the concentration of vanadium species is beyond a limit, the vanadium oxides in the polymerized form (extra framework) increase with further increases in vanadium concentration.

2.3. Identifying the isolated Fe-sites in Fe-zeolites

Fig. 8 displays the UV Raman spectra of three samples, silicalite-1, Fe-ZSM-5, and a mixture of silicalite-1 and Fe_2O_3. Silicalite-1 exhibits two bands at 380 and 802 cm^{-1}. The band at 380 cm^{-1} is assigned to the five-membered building unit of MFI-structure zeolites [40,41], and the 802 cm^{-1} band is assigned to the framework symmetric stretching vibration in ZSM-5 [2,4]. It is also interesting to note that Fe-ZSM-5 exhibits additional bands at 516, 580, 1026, 1126, and 1185 cm^{-1}. The chemical analysis of silicalite-1 and Fe-ZSM-5 shows that the iron is the

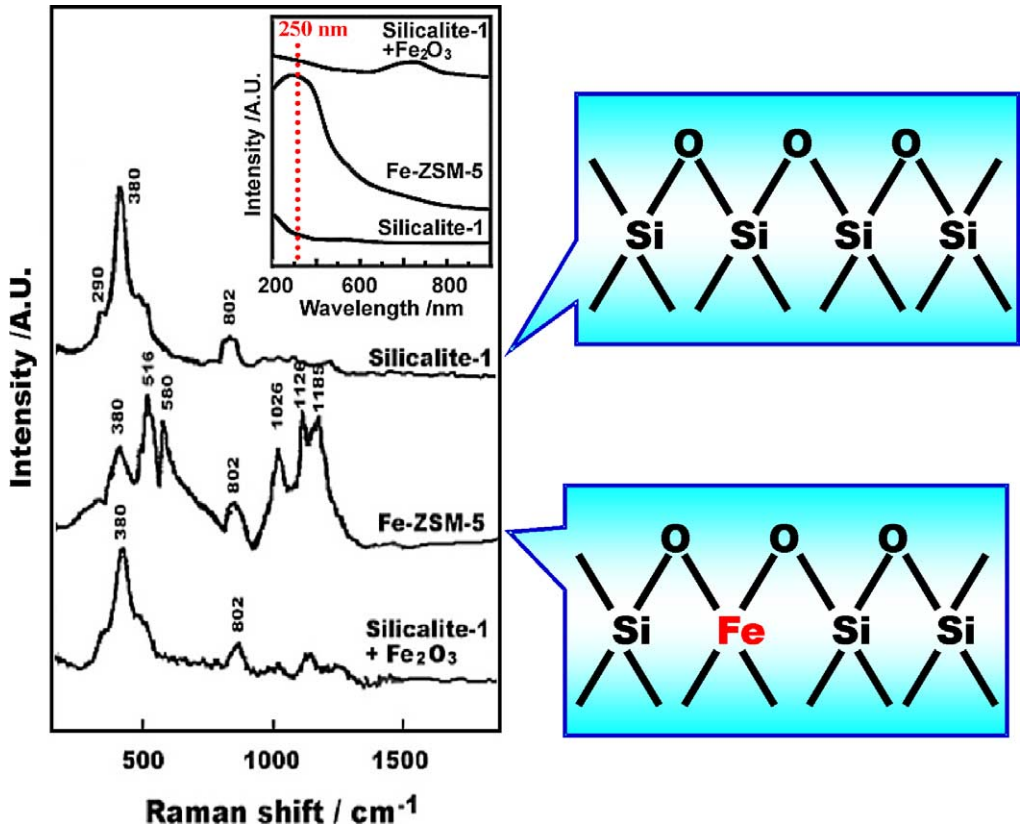

Fig. 6. UV Raman spectra ($\lambda_{ex} = 244$ nm) of Fe-ZSM-5, silicalite-1 and the mixture of silicalite-1 and Fe_2O_3. The inset presents the UV–visible diffuse absorbance of the three samples. The local structures of Fe-ZSM-5 and Silicalite-1 are schematically depicted.

only difference in chemical composition of these zeolites, and the new bands must therefore be attributed to the iron species. The UV Raman spectrum of the mechanical mixture of Fe_2O_3 with silicalite-1 gives bands similar to those of only silicalite-1. These results indicate that UV Raman spectroscopy using 244 nm as the excitation source is not sensitive to Fe_2O_3 material, and the Raman bands of Fe_2O_3 are not clearly observed [42].

The inset of Fig. 6 shows UV/Visible diffuse reflectance spectrum of silicalite-1, Fe-ZSM-5, and the mechanical mixture of Fe_2O_3 with silicalite-1. Silicalite-1 has no bands in the 200–700 nm region, while Fe-ZSM-5 shows a strong absorption band centered at 250 nm. The band at 250 nm is assigned to the $p\pi$–$d\pi$ charge-transfer transition between the iron and oxygen atoms in the framework of Fe–O–Si in the zeolite [43,44]. This is similar to the Ti–O–Si species of TS-1. The UV–visible diffuse reflectance spectrum of the mechanical mixture of Fe_2O_3 and silicalite-1 indicates that the absorption band in the UV region (200–300 nm) is very weak. The UV–visible diffuse reflectance spectra of silicalite-1 and ZSM-5 have no obvious absorption bands between 200 and 250 nm. The 244-nm laser used to excite the samples is close to the band center at 250 nm of Fe-ZSM-5, while the silicalite-1 and Fe_2O_3 have no electronic absorption band in the 250-nm region. Therefore, the UV Raman bands at 516, 580, 1026, and 1185 cm^{-1} are resonance Raman bands associated with the isolated iron species in the framework of Fe-ZSM-5, as depicted in the right panel of Fig. 6.

The Raman bands in the 516 cm^{-1} region are due to the symmetric stretching/bending vibrational modes of isolated Fe–O–Si species, while the bands at 1026, 1128, and 1185 cm^{-1} are attributed to the asymmetric vibrations of Fe–O–Si stretching vibrational modes [42]. The reason there are several bands in the 1100 cm^{-1} region is not well understood, but a detailed study is in progress. The split bands may suggest that there are several different kinds of highly isolated iron sites in Fe-ZSM-5. These bands evolve at different rates during the crystallization of Fe-ZSM-5, but the bands at 516 and 1026 cm^{-1} appear even at the very beginning of the crystallization. This allows us to conclude that the [≡Fe–O–Si≡]-like fragment species are derived even in the gel stage of the synthesis.

To better understand how much Fe can be incorporated in the framework, Fe–silicalite samples were prepared by hydrothermal synthesis with Fe_2O_3/SiO_2 molar ratios of 0.01, 0.005, 0.0025, and 0.00125 in the starting synthesis mixture. The as-synthesized samples were calcined in air at 773–823 K to remove the template and then washed by 0.1 M HCl to remove the extra framework iron oxide formed in the pores of the Fe–silicalite zeolite. Fig. 7 shows the UV Raman spectra of these Fe–silicalite samples with an excitation line at 244 nm. As seen in Fig. 6, the appearance of the two Raman bands at 380 and 800 cm^{-1} indicate the

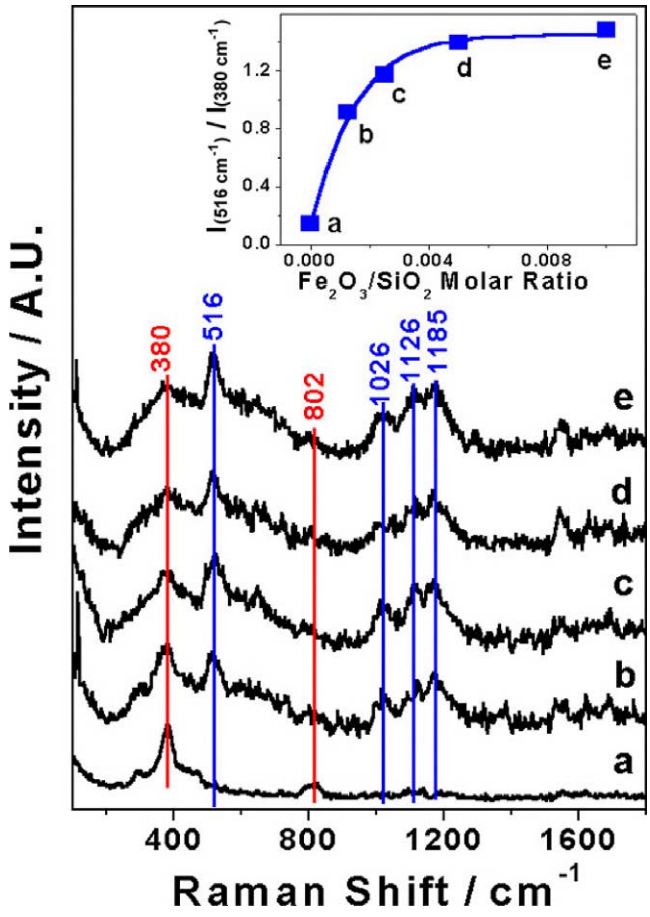

Fig. 7. UV Raman spectra ($\lambda_{ex} = 244$ nm) of Fe–silicalite synthesized with different Fe_2O_3/SiO_2 molar ratios of the starting materials. The inset gives the intensity ratio of the band at 516 cm^{-1} due to highly isolated Fe–O–Si species, and the band at 380 cm^{-1} (the characteristic Raman band of ZSM-5 as the internal standard) versus the Fe_2O_3/SiO_2 molar ratio (a, silicalite-1, $Fe_2O_3/SiO_2 = 0$; b, $Fe_2O_3/SiO_2 = 0.00125$; c, $Fe_2O_3/SiO_2 = 0.0025$; d, $Fe_2O_3/SiO_2 = 0.005$; e, $Fe_2O_3/SiO_2 = 0.01$).

formation of a silicalite-like structure in Fe–silicalite. The fact that the signal-to-noise ratio of the Raman spectra of Fe–silicalite is less than that of silicalite, particularly for the sample with a high Fe_2O_3/SiO_2 molar ratio, means that the crystalline quality of silicalite is deteriorated somewhat by the presence of iron species. The quality of the UV Raman spectrum can also be affected by the UV absorption of the extra framework iron oxide species.

The inset of Fig. 7 plots the intensity ratio of 516 to 380 cm^{-1} versus the Fe_2O_3/SiO_2 molar ratio. It is proposed that the intensity ratio of 516 to 380 cm^{-1} should be roughly proportional to the concentration of the isolated framework iron in Fe–silicalite when the concentration of iron species is very low. This intensity ratio linearly increases when the Fe_2O_3/SiO_2 ratio in the starting synthesis mixtures is increasing between 0 and 0.004. Then, the intensity ratio flattens when the Fe_2O_3/SiO_2 ratio is over 0.005. This result shows that the quantity of iron species being incorporated in the framework of silicalite is very small [45] and limited to a Fe_2O_3/SiO_2 ratio not greater than 0.005 for the samples synthesized in this work. However, the UV resonance Raman spectroscopy is able to identify extremely low concentrations of the isolated iron species in the zeolites.

3. Isolated and dispersed transition metal species on high surface area oxides

3.1. Molybdenum species on Al_2O_3

The supported molybdenum oxides have drawn a great deal of attention because they are the important catalysts and catalyst precursors used in many chemical reactions. However, past Raman spectroscopic studies on the supported molybdate mainly focused on high loading catalysts. The molybdenum oxides are usually in the aggregated/polymerized form or even in the bulk oxide form on the alumina surfaces when the loading of molybdenum oxide is high. One may not only detect isolated transition metal oxides but also understand the coordination and interaction between the metal oxides and the support surfaces when the loading is sufficiently low. For the low loading catalyst, it is difficult to obtain its Raman spectrum because of the fluorescence and the relatively low sensitivity of conventional Raman spectroscopy. Fortunately, UV resonance Raman spectroscopy presents the possibility of being able to detect the surface species with low concentration.

Fig. 8 shows the UV Raman spectra of supported molybdate on γ-alumina (MoO_3/γ-Al_2O_3) with extremely low loading (0.10 wt% MoO_3, about 0.007 monolayer of γ-Al_2O_3, $S_{BET} = 250$ m^2/g) [46]. Fig. 8a presents only the strong fluorescence when the sample was excited by the visible laser at 488 nm. The Raman spectrum is greatly improved when the excitation laser is shifted from 488 to 325 nm, and the Raman bands at 325, 837, 910, and 1670 cm^{-1} can be observed despite some fluorescence (Fig. 8b). The fluorescence is completely removed when the excitation laser is shifted to the UV region as clearly shown in Fig. 8c. These results again demonstrate that the intensity of the fluorescence band decreases as the wavelength approaches the UV region (Fig. 1).

The Raman bands in Figs. 8b and 8c are clearly detected owing to not only the avoidance of fluorescence but also the resonance Raman enhancement. As seen in the inset, there are two absorbances centered at 220 and 290 nm for MoO_3/γ-Al_2O_3. The band at 220 nm is mainly associated with the tetrahedral molybdate species and the band at 290 nm is associated with the octahedral molybdate species. The laser at 325 nm is close to the band at 290 nm, so that the resonance Raman effect enhances the Raman bands at 837 and 1670 cm^{-1} of octahedral species (asymmetric vibration of Mo–O–Mo). The appearance of the overtone band at 1670 cm^{-1} (of the band at 837 cm^{-1}) also suggests the presence of the resonance Raman effect. The band at 910 cm^{-1} (stretching vibration of Mo=O) due to the tetrahedral species is observed possibly also due to the

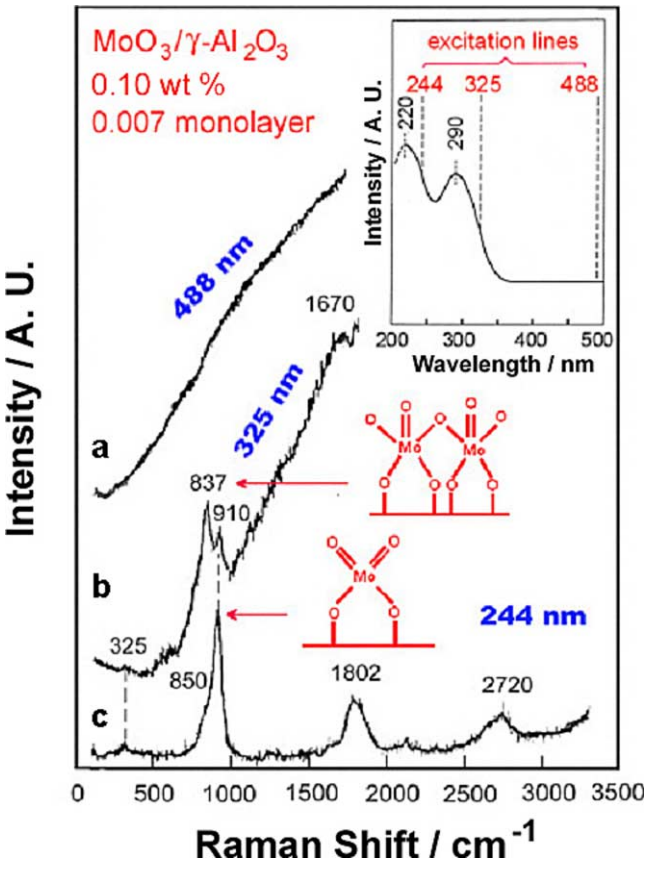

Fig. 8. Raman spectra of MoO_3/γ-Al_2O_3 excited by different lasers at 244, 325, and 488 nm. The inset is the UV–visible diffuse absorbances of MoO_3/γ-Al_2O_3, where two absorbances at 229 and 290 nm are associated with the isolated and polymerized molybdate species, respectively. The lasers at 244 and 325 nm are in the regions of 229 and 290 nm, respectively, so the preresonance Raman effect is observed.

resonance Raman effect because the surface concentration of either octahedral or tetrahedral species is very low.

The resonance Raman effect becomes even more obvious in Fig. 8c, where the band at 910 cm^{-1} and its overtones at 1802 and 2720 cm^{-1} are clearly detected. The Raman bands of tetrahedral species are selectively enhanced because the laser at 244 nm is near to the absorbance band at 220 nm of the tetrahedral species. This unambiguously confirms the assignment of the Raman bands of different surface species based on the resonance Raman effect. It is worthwhile to note that the polymerized (octahedral) species are still formed along with the isolated (tetrahedral) species on the Al_2O_3 surface even at a low loading of MoO_3 (0.10 wt%).

The molybdate species on the alumina surface were prepared by a chemical equilibrium adsorption method in order to make more isolated species. UV Raman spectra show that the species absorbed on the support in a wet state are not always in agreement with those in an impregnation solution [47]. The state of the surface molybdate species in the wet state is determined by both the pH value of the impregnating solution and the pH value at PZC (the point of zero charge) of the support. During calcination of the catalyst prepared with $(NH_4)_6Mo_7O_{24}$ some tetrahedral molybdate species aggregate into the octahedral species. This can be explained by the decrease in the surface acidity when NH_3 runs away from the surface. The tetrahedral molybdate species do not polymerize when the catalyst is prepared with a solution of $NaMoO_4$ because the surface acidity hardly changes during calcination [48]. The surface acidity of the catalyst, which is influenced by the pH value of the impregnating solution, the pH value at PZC of the support, molybdenum loading, and compensatory cations, is a crucial factor for controlling the coordination structure of the surface molybdate species.

3.2. *Titanium species on SiO_2*

Highly dispersed titanium species on silica (Ti/SiO_2) were prepared by chemical grafting using $TiCl_4$ and tetraethyl othosilicate as the precursors and SiO_2 as the support [49]. The catalysts were tested for the epoxidation of styrene using *tert*-butyl hydroperoxide (TBHP) as the oxidant. Fig. 9 (left panel) shows the catalytic performance of the catalysts prepared at different grafting temperatures. Catalysts prepared at high grafting temperatures demonstrate high epoxide selectivity. The conversion does not significantly change for these different catalysts, and the selectivity of benzaldehyde decreases with the grafting temperatures. This indicates that the number of active sites for epoxidation (usually the isolated titanium sites) increases at higher grafting temperatures.

Fig. 9 (right panel) shows the UV Raman spectra of the Ti/SiO_2 catalysts prepared by chemical grafting at different temperatures. The excitation laser at 244 nm is close to the electronic absorption band of isolated titanium ions tetrahedrally coordinated. The resonance Raman bands at 532 and 1085 cm^{-1} are readily attributed to the isolated titanium ions in tetrahedral coordination as in TS-1. It is interesting that the bands at 532 and 1085 cm^{-1} develop with higher grafting temperatures. This strongly suggests that the formation of isolated titanium species require higher grafting temperatures. Correlating the Raman bands with the catalytic properties shown in the left panel proves that the isolated surface titanium species are mainly responsible for the epoxidation selectivity.

The two characteristic Raman bands at 532 and 1085 cm^{-1} of isolated titanium species on the SiO_2 surface are analogous to those bands at 490, 530, and 1125 cm^{-1} of TS-1 (Fig. 4). This implies that the isolated titanium sites of Ti/SiO_2 resemble the isolated framework titanium sites in TS-1. One interesting difference is that the characteristic band at 1085 cm^{-1} due to the asymmetric vibration of Ti–O–Si is about 40 cm^{-1} lower than that in TS-1 (1125 cm^{-1}, see Fig. 4). We also found that this band for Ti-MCM-41 and Ti-SBA is between 1100 and 1110 cm^{-1} [50–52], always lower than 1125 cm^{-1}. This difference in frequency essentially reflects the different coordination of titanium ions. In TS-1, the titanium ion is in the rigid tetrahedral coordination,

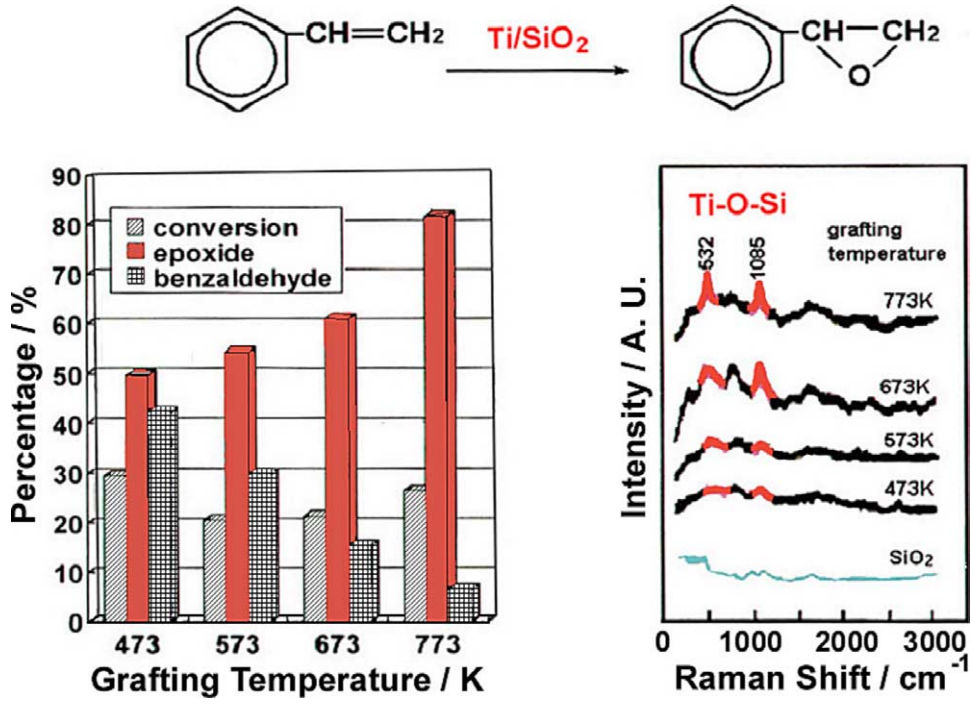

Fig. 9. (Left panel) The conversion and selectivity of styrene epoxidation on Ti/SiO_2 catalysts prepared by chemically grafting the $TiCl_4$ on silica at different temperatures (the synthesized samples were carefully treated with diluted steam). (Right panel) UV Raman spectra ($\lambda_{ex} = 244$ nm) of the as-synthesized Ti/SiO_2 catalysts. The Raman bands at 532 and 1085 cm^{-1} are due to the highly isolated titanium species of Ti/SiO_2 catalysts.

as a consequence giving the highest vibrational frequency of Ti–O–Si at 1125 cm^{-1}. While in Ti/SiO_2 and Ti-MCM-41, the titanium species are in a relatively flexible coordination on the surface of silica. Accordingly, the asymmetric vibration of Ti–O–Si shifts to lower frequency. In fact, this red shift is an indication of the coordination environment of isolated titanium ions.

4. Concluding remarks and prospects

UV Raman spectroscopy broadens the applications of Raman spectroscopy in catalysis by avoiding the fluorescence and improving the sensitivity. UV resonance Raman spectroscopy is very sensitive and supplies more information about the active sites of catalysts. In particular, the isolated transition metal ions/oxides with extremely low concentration in the framework of molecular sieves and on oxide supports can be identified by the UV resonance Raman spectroscopy. Preparing the uniformly distributed and well-designed isolated active sites is crucial to achieving high activity and selectivity. Building up the relationship between the structure of the catalyst and catalytic performance is based on the understanding of the structure of active sites and their surroundings. It is possible to tune the coordination structure and to test the activity and selectivity of the isolated sites. If one definitely characterizes the structure, it could be helpful for understanding early stage the fundamental issues of catalysis.

The in-situ characterization of catalytic materials during their synthesis/preparation is very important in understanding how the active sites evolve and what are the key steps in generating the structure of active sites. Raman spectroscopy is a suitable tool for characterizing the catalyst preparation from the early stage of the synthesis, such as aqueous solution and gel, to the solid states after successive steps of treatment, such as drying and calcination [53].

The in-situ characterization of catalytic reactions has received a great deal of attention, and UV Raman spectroscopy can be widely used to detect the surface species derived during the reactions. Progress was recently made by Peter Stair's group, who used a specially designed Raman cell to realize the in-situ UV Raman study of a catalytic reaction [54,55]. The samples in the cell are constantly moving during the measurement and the laser always meets the fresh catalyst, so that the possible thermal/photo decomposition of surface species caused by UV laser could be avoided. It is also worthwhile to note that the surface species and the active sites might be in a dynamic state under reaction conditions, so to characterize the catalyst with time-resolved Raman spectroscopy is absolutely necessary.

Spectroscopic characterization combined with theoretical calculation will be very helpful in the elucidation of the local structure of the active sites and of the active sites under reaction conditions. It is now possible to calculate the spectroscopic results by using theoretical calculations, such as Hartee–Fock, density functional theory, and molecular dynamics [31,56–59].

Acknowledgments

The author acknowledges his colleagues who contributed to this study, among them are Guang Xiong, Zhaochi Feng, Yi Yu, Qihua Yang, Pinliang Ying, Bo Han, and Qin Xin. The discussion with Peter Stair at Northwestern University was also very helpful. This work was financially supported by the National Natural Science Foundation of China (NSFC Grants 20073045, 20172051, and 20273070) and the National Project from the Ministry of Science and Technology of China (Grant G1999022407).

References

[1] I.R. Lewis, H.G.M. Edwards (Eds.), Handbook of Raman Spectroscopy, Dekker, New York, 2001.
[2] C. Li, P.C. Stair, Catal. Lett. 36 (1995) 119.
[3] C. Li, P.C. Stair, Stud. Surf. Sci. Catal. 101 (1996) 881.
[4] C. Li, P.C. Stair, Catal. Today 33 (1997) 353.
[5] P.C. Stair, C. Li, J. Vac. Sci. Technol. A 15 (1997) 1679.
[6] C. Li, P.C. Stair, Stud. Surf. Sci. Catal. 105 (1997) 599.
[7] G. Xiong, C. Li, Z.-C. Feng, P.-L. Ying, Q. Xin, J.-K. Liu, J. Catal. 186 (1999) 234.
[8] J. Li, G. Xiong, Z.-C. Feng, Z.-M. Liu, Q. Xin, C. Li, Micropor. Macropor. Mater. 39 (2000) 275.
[9] K. Nakamoto, Infrared and Raman Spectra of Inorganic and Coordination Compounds, Wiley, New York, 1978.
[10] W. Holderich, M. Messe, M. Nauman, Angew. Chem. Int. Ed. Engl. 27 (1988) 226.
[11] J.A. Martens, Ph. Buskens, P.A. Jacobs, Appl. Catal. A 99 (1993) 71.
[12] L.J. Burcham, M. Badlani, I.E. Wachs, J. Catal. 203 (2001) 104.
[13] U.-A. Schubert, F. Anderle, J. Spengler, J. Zuhlke, H.-J. Eberle, R.K. Grasselli, H. Knozinger, Top. Catal. 15 (2001) 195.
[14] A. Tuel, Zeolites 16 (1996) 108.
[15] L. Tosheva, B. Mihailova, V. Valtchev, J. Sterte, Micropor. Mesopor. Mater. 39 (2000) 91.
[16] D. Scarano, A. Zecchina, S. Bordiga, F. Geobaldo, G. Spoto, J. Chem. Soc., Faraday Trans. 89 (1993) 4123.
[17] A.J.H.P. Van der Pol, A.J. Verduyn, J.H.C. van Hooff, Appl. Catal. 92 (1992) 113.
[18] P. Behrens, J. Felsche, S. Vetter, G. Schulz-Ekloff, N.I. Jaeger, W. Niemann, J. Chem. Soc., Chem. Commun. (1991) 678.
[19] A. Tuel, Y. Ben Taarit, Zeolites 14 (1994) 169.
[20] C. Lamberti, S. Bordiga, A. Zecchina, A. Carati, A.N. Fitch, G. Artioli, G. Petrini, M. Salvalaggio, G.L. Marra, J. Catal. 183 (1999) 222.
[21] C. Lamberti, S. Bordiga, A. Zecchina, G. Artioli, G. Marra, G. Spano, J. Am. Chem. Soc. 123 (2001) 2204.
[22] A.J.M. De Man, J. Phys. Chem. 100 (1996) 5025.
[23] R.M. Boccuti, K.M. Rao, A. Zecchina, Stud. Surf. Sci. Catal. 48 (1989) 133.
[24] M.A. Camblo, A. Corma, J. Perez-Pariente, J. Chem. Soc., Chem. Commun. (1993) 557.
[25] C. Li, G. Xiong, Q. Xin, J.-K. Liu, P.-L. Ying, Z.-C. Feng, J. Li, W.-B. Yang, Y.-Z. Yang, G.-R. Wang, X.-Y. Liu, M. Lin, X.-Q. Wang, E.-Z. Min, Angew. Chem. Int. Ed. 38 (1999) 2220.
[26] C. Li, G. Xiong, Q. Xin, J.-K. Liu, P.-L. Ying, Z.-C. Feng, J. Phys. Chem. B 105 (2001) 2993.
[27] E. Astorino, J.B. Peri, R.J. Willey, G. Busca, J. Catal. 157 (1995) 482.
[28] G. Busca, G. Ramis, J.M. Gallarado Amores, V.S. Escribano, P. Piaggio, J. Chem. Soc., Faraday Trans. 90 (1994) 3181.
[29] A. Zecchina, G. Spoto, S. Bordiga, A. Ferrero, G. Petrini, G. Leofanti, M. Padovan, Zeol. Chem. Catal. 251 (1991) 671.
[30] L.D. Ziegler, Acc. Chem. Res. 27 (1994) 1.
[31] G. Ricchiardi, A. Damin, S. Bordiga, C. Lamberti, G. Spano, F. Rivetti, A. Zecchina, J. Am. Chem. Soc. 123 (2001) 11409.
[32] G. Xiong, C. Li, H.Y. Li, Q. Xin, Z.-C. Feng, Chem. Commun. (2000) 677.
[33] T. Sen, V. Ramaswamy, S. Ganapathy, P.R. Rajamohanan, S. Sivasanker, J. Phys. Chem. 100 (1996) 3809.
[34] K.J. Chao, C.N. Wu, H. Chang, L.J. Lee, S.F. Hu, J. Phys. Chem. 101 (1997) 6341.
[35] Z.H. Luan, J. Xu, H.Y. He, J. Klinowski, L. Kevan, J. Phys. Chem. 100 (1996) 19595.
[36] G.T. Centi, S. Perathoner, F. Trifire, A. Aboukais, C.F. Aissi, M. Guelto, J. Phys. Chem. 96 (1992) 2617.
[37] C. Cristiani, P. Forzatti, G. Busca, J. Catal. 116 (1989) 586.
[38] H. Selig, H.H. Claassen, J. Chem. Phys. 44 (1996) 1404.
[39] G.T. Went, S.T. Oyama, A.T. Bell, J. Phys. Chem. 94 (1990) 4240.
[40] P.K. Dutta, M. Puri, J. Phys. Chem. 91 (1987) 4329.
[41] P.K. Dutta, K.M. Rao, J.Y. Park, J. Phys. Chem. 95 (1991) 6645.
[42] Y. Yu, G. Xiong, C. Li, F.-S. Xiao, J. Catal. 194 (2000) 487.
[43] B.N. Figgis, Introduction to Ligand Field, Wiley, New York, 1996.
[44] S. Bordiga, R. Ruzzoni, F. Geobaldo, C. Lamberti, E. Giamello, A. Zecchina, G. Leofanti, G. Petrini, G. Tozzola, G. Vlaic, J. Catal. 158 (1996) 486.
[45] R. Szostak, V. Nair, T.L. Thomas, J. Chem. Soc., Faraday Trans. I 83 (1987) 487.
[46] Y.-C. Xie, Y.-Q. Tang, Adv. Catal. 37 (1990) 1.
[47] Y. Iwasawa, M. Yamagishi, J. Catal. 82 (1983) 373.
[48] G. Xiong, Z.-C. Feng, J. Li, Q.-H. Yang, P.-L. Ying, Q. Xin, C. Li, J. Phys. Chem. 104 (2000) 3581.
[49] Q.-H. Yang, S.-L. Wang, J.-Q. Lu, G. Xiong, Z.-C. Feng, Q. Xin, C. Li, Appl. Catal. A 194–195 (2000) 507.
[50] J.-Q. Yu, Z.-C. Feng, L. Xu, M.-J. Li, Q. Xin, Z.-M. Liu, C. Li, Chem. Mater. 13 (2001) 994.
[51] Z.-T. Zhang, Y. Han, F.-S. Xiao, S.-L. Qiu, L. Zhu, R.-W. Wang, Y. Yu, Z. Zhang, B.-S. Zou, Y. Wang, H.-P. Sun, D.-Y. Zhao, Y. Wei, J. Am. Chem. Soc. 123 (2001) 5014.
[52] W.-H. Zhang, J.-Q. Lu, B. Han, M.-J. Li, J.-H. Xiu, P.-L. Ying, C. Li, Chem. Mater. 14 (2002) 3413.
[53] A.M. Rzhevskii, P. Choi, F.H. Ribeiro, R.J. Gulotty, M.M. Olken, Catal. Lett. 73 (2001) 187.
[54] Z.-X. Gao, H.-S. Kim, Q. Sun, P.C. Stair, W.M. Sachtler, J. Phys. Chem. B 105 (2001) 6186.
[55] P.C. Stair, Current Opinion Solid State Mater. Sci. 5 (2001) 365.
[56] A.L. Yakovlev, G.M. Zhidomirov, R.A. van Santen, J. Phys. Chem. B 105 (2001) 12297.
[57] G. Sankar, J.M. Thomas, A.R.A. Catlow, C.M. Barker, D. Gleeson, N. Kaltsoyannis, J. Phys. Chem. B 105 (2001) 9028.
[58] J.E. Sponer, Z. Sobalik, J. Leszczynski, B. Wichterlova, J. Phys. Chem. B 105 (2001) 8285.
[59] R. Radhakrishnan, C. Reed, S.T. Oyama, M. Seman, J.N. Kondo, K. Domen, Y. Ohminami, K. Asakura, J. Phys. Chem. B 105 (2001) 8519.